BMC Chemistry

RESEARCH

Open Access

Utilizing MEDT analysis of [3+2] cycloaddition reaction: x-ray crystallography of spirooxindole linked with thiophene/furan heterocycles and triazole framework

Abdulmajeed Abdullah Alayyaf[1], M. Ali[1], Moayad Abdullah Alwehaibi[1], Muhanna K. Al-Muhanna[2], Saied M. Soliman[3], Mar Ríos-Gutiérrez[4], Matti Haukka[5] and Assem Barakat[1*]

Abstract

Hybridization of spirooxindole with different pharmacophores such as triazole and heterocycle such as thiophene and furan moiety was achieved by the [3+2] cycloaddition (32CA) reaction approach. Structural investigations of the compounds **4a** and **4b** were performed using X-ray single crystal structure determinations and Hirshfeld analysis. Both compounds crystallized in monoclinic crystal system. The space group is $P2_1/c$ for **4a** and $P2_1/n$ for **4b**. The crystal parameters are $a=10.2619(3)$ Å, $b=13.6776(3)$ Å, $c=10.9318(3)$, $\beta=116.640(4)°$ for the former while $a=13.0012(1)$ Å, $b=14.9692(1)$ Å, $c=14.1178(1)$ Å, $\beta=97.101(1)°$ for the latter. In both compounds, the aryl group and the triazole moieties are twisted from one another. The twist angle is 84.75˚for **4a** while 86.64˚ for **4b**. Based on Hirshfeld calculations, the Cl…H, O…H, N…H and C…H non-covalent interactions in **4a** while the O…H interactions in **4b** are the most important. The molecular mechanism of the key 32CA reaction between the in situ generated azomethine ylides and the corresponding chalcones has been studied within the Molecular Electron Density Theory (MEDT). The MEDT study reveals that the low activation energies and high experimental selectivity are the result of the supernucleophilic character of the ylides and the strong electrophilicity of the chalcones, which favour the process through a high polar character. This high polar character accounts for the total *endo* selectivity experimentally found.

Keywords Spirooxindoles, Triazole, Heterocycle, Molecular Electron Density Theory (MEDT)

*Correspondence:
Assem Barakat
ambarakat@ksu.edu.sa
[1]Department of Chemistry, College of Science, King Saud University, P. O. Box 2455, Riyadh 11451, Saudi Arabia
[2]The Material Science Research Institute, King Abdulaziz City for Science and Technology (KACST), Riyadh 11442, Saudi Arabia
[3]Department of Chemistry, Faculty of Science, Alexandria University, P.O. Box 426, Ibrahimia, Alexandria 21321, Egypt
[4]Department of Organic Chemistry, University of Valencia, Dr. Moliner 50, Burjassot, Valencia 46100, Spain
[5]Department of Chemistry, University of Jyväskylä, P.O. Box 35, Jyväskylä FI-40014, Finland

Introduction

The field of diversity-oriented and combination organic syntheses, which focuses on the construction of heterocyclic hybrids possessing various structural features and significant pharmacological relevance, has garnered considerable interest in recent decades. The chemical industry and scientific community face a significant challenge in applying readily available initial substances in a way that adheres to atom economics and environmental considerations [1].

The synthesis of spiro-hybrid heterocycles has attracted considerable attention from both chemists and medicinal/pharmaceutical researchers. This is due to the significant importance of these compounds in various fields, including but not limited to, drug discovery, material sciences, and organic synthesis. The spiro-hybrid heterocyclic framework offers unique structural features and diverse physicochemical properties, making them attractive targets for the design and development of novel compounds with potential applications in the pharmaceutical and chemical industries.

The multi-component reaction (MCR) approach is preferred for constructing spirohybrids. It enables researchers to create diverse heterocycles in a single process, with fewer workup steps, easy mechanization, and simple purification. This method is eco-friendly, reproducible and follows the principle of atom economy [2, 3]. Specifically, heterocycles of spiropyrrolidine are found in natural and synthetic compounds, exhibiting important pharmacological properties. They can be produced through a [3+2] cycloaddition mechanism involving multi-component reactions (MCRs) [4–6] Numerous naturally occurring alkaloids, such as horsfiline, contain the spiropyrrolidine structural motif and have been used in traditional medicine [7]. It has been reported that spirotryprostatine A and B [8], as well as mitraphylline, are highly effective anti-cancer agents [9]. A large number of synthetic spiropyrrolidines analogs have been synthesized and evaluated against various targets, including cancer activity, in addition to naturally occurring compounds [10, 11], local anesthetics [12], analgesic and anti-inflammation [13] and other activity, such as antimycobacterial [14] and anti-microbial agents [15], and others [16–22].

The 1,2,3-triazole unit has potential pharmacological application [23], like being a carbonic anhydrase inhibitor, and is widely studied in synthetic chemistry [24], treatment of tuberculosis [25–27] and agent of antimalarial [27] and others.

Organic chemists have extensively studied the electronic structure of three-atom components (TACs) that are generated in situ as intermediates in 32CA reactions. These studies have been aided by the Molecular Electron Density Theory (MEDT) [28]. Four different types of three-atom-components (TACs) have been characterized, namely *zwitterionic (zw)*,*carbenoid (cb)*,*pseudo(mono)radical (pmr)*,*and pseudodiradical (pdr)* TACs, and an excellent structure/reactivity relationship was found towards ethylene [29]. It is worth mentioning that *pseudo(mono)radical* and *pseudodiradical* TACs exhibit high reactivity as a result of their inherent instability. The electronic configurations and associated reactivities can be altered through the process of substitution.

Pyrrolidines are a group of heterocyclic compounds characterized by five-membered rings. These compounds play a crucial role in drug design due to their significant pharmacological relevance [30–32]. Pyrrolidines can be readily synthesized through the 32CA reaction of azomethine ylides (AYs) with olefins. The process of drug design often involves adding a spiro-ring to heterocyclic compounds to restrict their conformation. Spirooxindoles are formed when exocyclic AY, which is derived from a dicarbonyl molecule called isatin, interacts with other compounds. These spirooxindoles have significant pharmacological effects [10, 21, 33, 34].

As part of our ongoing research program [35, 36], we are exploring multi-component reactions for synthesizing functionalized molecules with distinct pharmacophores, including spiropyrrolidine, 1,2,3-triazole unit, and heterocycles scaffold within a single compound. Our previous results have shown promising outcomes in this field. Such compounds could be crucial in the field of drug discovery and may have significant importance. In this study, we present a novel series of spiropyrrolidine analogs, synthesized, characterized, and analyzed via X-ray structure. Additionally, we provide mechanistic insights into the 32CA reaction method based on the MEDT [28].

Results and discussion

The synthesis of spirooxindole hybrids incorporating heterocycle such as thiophene and furan moiety conjugated with triazole scaffold was achieved using the 32CA reaction approach, as illustrated in Scheme 1 and following a previously described method [22]. The requested ethylene derivatives **1a**,**b** for this 32CA reaction was synthezied according to our described method [22]. To achieve the 32CA method, the process involves generating in situ azomethine ylides (AYs) by reacting isatin derivatives (**2a**,**b**) with L-proline (**3**). Subsequently, the AYs were reacted with ethylene derivatives **1a**,**b**, leading to the formation of the novel spirooxindole compounds **4a**,**b**. This synthetic process resulted in the creation of asymmetric molecules with four chiral centers in a regio- and diastereoselective manner and high chemical yield.

The complexity of the molecular structure of the synthesized spirooxindoles was confirmed through NMR

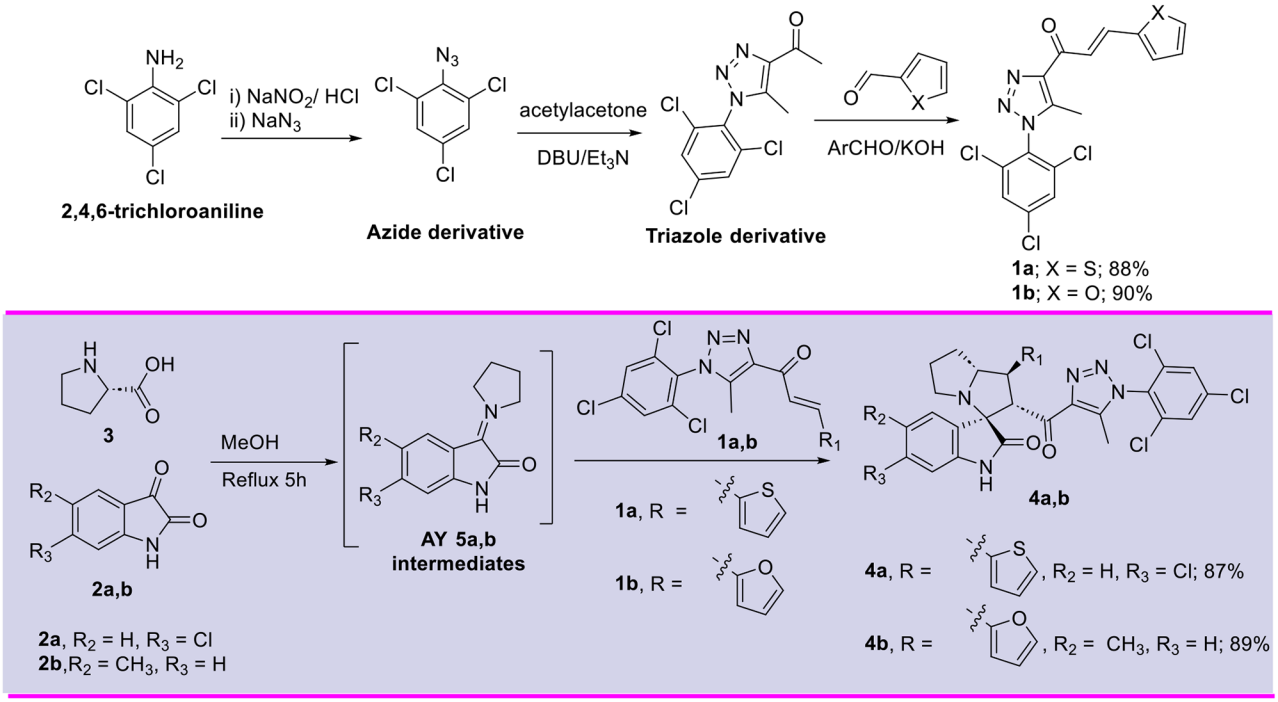

Scheme 1 Synthesis of the spirooxindoles **4a**,**b**

spectroscopic analyses (see Supplementary Materials), which matched the proposed structures. As an example the ^{1}H-NMR of the spirooxindole **4a** has shown the expected protons as follow: δ 10.28 (s, 1H) assigned for the secondary amine proton; the aromatic region 7.99–6.48 ppm were assigned for the aromatic protons including the heterocyles protons; then fused rings protons and the methyl group of the triazole ring was assigned in the aliphatic region. The ^{13}C-NMR sectrum data shown the expected carbons. Additionally, two crystalline compounds were successfully obtained, and their structures were definitively determined through single-crystal X-ray diffraction analysis. The mechanism underlying this synthesis process adhered to a regiospecific and diastereospecific pathway, consistent with previously reported literature. In this pathway, the 32CA reaction proceeded through an *ortho/endo* mechanism in a two-stage one-step process.

Crystal structure description

Further characterization for the structure of the studied compounds was performed by obtaining single crystals from the target compounds then determining their single crystal X-ray structures. For **4a**, the X-ray structure is presented in Fig. 1. The crystal system for **4a** is monoclinic while space group is *P2(1) (No. 4)*. The unit cell parameters are a=10.2619(3) Å, b=13.6776(3) Å, c=10.9318(3), β=116.640(4)°. There is one molecule of **4a** in the asymmetric unit while z=2. Other crystal data details are depicted in Table 1. For example, the crystal density is 1.534 mg/m^3 and the unit cell volume is 1371.48(8) Å^3. The X-ray structure confirmed with no doubt the engagement of the different bioactive moieties in on organic hybrid. The phenyl group attached to the triazole ring is almost located perpendicular to it. The angle between their mean planes is 84.75°. Some selected bond distances and angles are given in Table S1 (Supplementary data).

The molecular packing of **4a** is dominated by strong N(4)-H(4)…O(1) hydrogen bonds in addition to the weak C(4)-H(**4a**)…O(2), C(21)-H(21B)…Cl(4) and C(23)-H(23)…Cl(3) interactions. The H(4)…O(1) distance is 2.13(4) Å while the H(**4a**)…O(2), H(21B)…Cl(4) and H(23)…Cl(3) distances are 2.38, 2.87 and 2.81 Å, respectively. Details about the geometric parameters of these non-covalent interactions are listed in Table 2. While presentation of the different contacts and hyydrogen bond packing scheme is shown in Fig. 2.

For **4b**, the structure is confirmed using single crystal X-ray crystallography as shown in Fig. 3. Similar to **4a**, the compound **4b** crystallized in the same crystal system and $P2_1/n$ space group. The lattice parameters are a=13.0012(1) Å, b=14.9692(1) Å, c=14.1178(1) Å, β=97.101(1)°. The asymmetric unit contains one molecule of **4b** while z=4 (Table 1). The crystal density is 1.454 Mg/m^3 and the unit cell volume is 2726.50(3) Å^3. In this case, the aryl group and the triazole moieties make

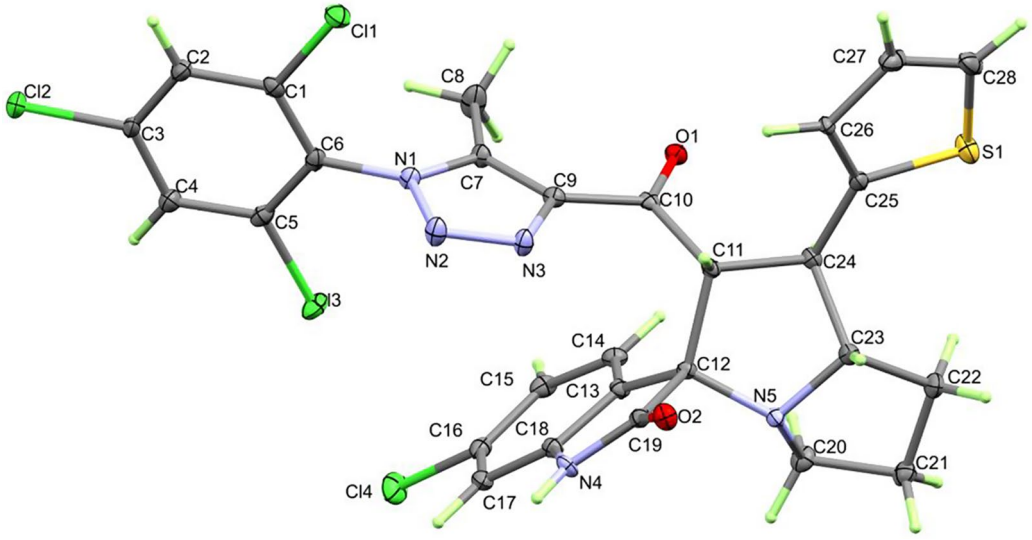

Fig. 1 X-ray structure of **4a**. The displacement ellipsoids are drawn at 50% probability level

Table 1 Crystal data

	4a	4b
CCDC	2,303,110	2,303,111
empirical formula	$C_{28}H_{21}Cl_4N_5O_2S$	$C_{29}H_{24}Cl_3N_5O_3$
fw	633.36	596.88
temp (K)	120(2)	120(2)
λ(Å)	0.71073	0.71073
cryst syst	Monoclinic	Monoclinic
space group	$P2_1$	$P2_1/n$
a (Å)	10.2619(3)	13.0012(1)
b (Å)	13.6776(3)	14.9692(1)
c (Å)	10.9318(3)	14.1178(1)
β (deg)	116.640(4)	97.101(1)
V (Å^3)	1371.48(8)	2726.50(3)
Z	2	4
ρ_{calc} (Mg/m^3)	1.534	1.454
μ(Mo Kα) (mm^{-1})	0.546	0.378
No. reflns.	13,579	73,326
Unique reflns.	7380	11,390
Completeness to θ = 25.242°	100%	99.9%
GOOF (F^2)	1.030	1.043
R_{int}	0.0265	0.0354
R_1[a] ($I \geq 2\sigma$)	0.0373	0.0422
wR_2[b] ($I \geq 2\sigma$)	0.0770	0.1081
Absolute structure parameter	-0.01(2)	

[a] $R_1 = \Sigma||F_o| - |F_c||/\Sigma|F_o|$

[b] $wR_2 = \{\Sigma[w(F_o^2 - F_c^2)^2]/\Sigma[w(F_o^2)^2]\}^{1/2}$

an angle of 86.64° which also indicated the perpendicularity of the two ring on each other.

The molecules of **4b** are packed in the three dimensional via N(6)-H(6)…N(2) hydrogen bonds and the non-classical C(2)-H(2)…O(1) interaction. The H(6)…N(2) and H(2)…O(1) distances are 2.52(2) and 2.24 Å, respectively while the N(6)…N(2) and C(2)…O(1) distances are 3.267(2) and 3.152(1) Å. Presentation of these contacts and their geometric details are presented in Fig. 4a; Table 2.

Table 2 Hydrogen bonds for **4a** and **4b** [Å and °]

D-H…A	d(D-H)	d(H…A)	d(D…A)	< (DHA)	Symm. Code
4a					
N(4)-H(4)…O(1)	0.79(4)	2.13(4)	2.901(3)	167(3)	-x + 1,y-1/2,-z + 1
C(4)-H(**4a**)…O(2)	0.95	2.38	3.308(4)	166	x, y,z-1
C(21)-H(21B)…Cl(4)	0.99	2.87	3.681(3)	140.2	x, y,z + 1
C(23)-H(23)…Cl(3)	1.00	2.81	3.730(3)	152.9	x, y,z + 1
4b					
C(2)-H(2)…O(1)	0.95	2.24	3.152(1)	160	-x + 3/2,y-1/2,-z + 3/2
N(6)-H(6)…N(2)	0.92(2)	2.52(2)	3.267(2)	139.5(18)	-x + 1,-y,-z + 1

Hirshfeld surface analysis

In order to shed the light on the detailed supramolecular structure aspects of the studied compounds, Hirshfeld topology analysis was performed. The resulting mapped surfaces for **4a** are presented in Fig. 5. Different red spots were observed at the d_{norm} map are found related to the Cl…H, O…H, N…H and C…H non-covalent interactions. These contacts appeared as short interactions with distances shorter than the vdWs radii sum of the interacting atoms. In this crystal structure, no evidences from the curvedness and shape index about the presence of π-π stacking interactions.

On the other hand, the analysis of the fingerprint plots gave indication on the percentages of all possible contacts in the crystals structure. These interactions and their percentages are presented in Fig. 6. The major contacts are

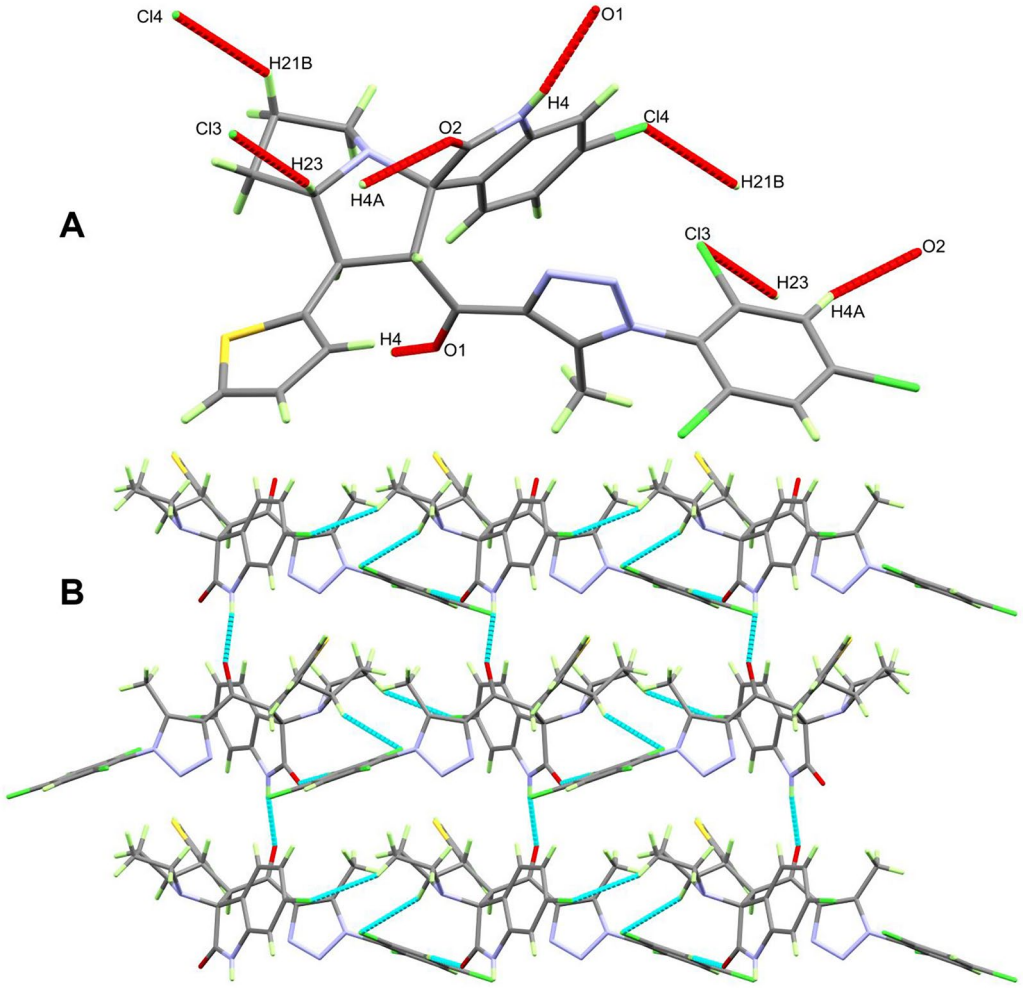

Fig. 2 The important contacts (**A**) and H-bond scheme (**B**) for **4a**

the H…H and Cl…H interactions which represent more than half the amount of all other contacts. The percentages of the most important contacts are 25.4%, 10.3%, 7.1% and 13.9% the Cl…H, O…H, N…H and C…H non-covalent interactions, respectively. There are many other contacts were detected in this crystal structure, but all have small percentages and appeared as blue regions in the d_{norm} map. Hence are considered less important and weak compared to the Cl…H, O…H, N…H and C…H non-covalent interactions.

In addition, careful inspection for the decomposed fingerprint plots of the Cl…H, O…H, N…H and C…H non-covalent interactions further revealed the importance of these contacts in the molecular packing. All these contacts appeared either as sharp spikes or wing which is the characteristic features of short interactions which have great significance in the supramolecular structure of **4a** (Fig. 7). Summary of the short contacts and the respective interaction distances are presented in Table 3. The Cl3…H23, O1…H4, N2…H28 and C6…H21A are the shortest non-covalent interactions detected in this crystal structure. Their interaction distances are 2.738, 1.912, 2.59 and 2.691 Å, respectively where all have shorter distances than the vdWs radii sum of the interacting atoms.

For the compound **4b**, the Hirshfeld mapped surfaces are shown in Fig. 8. It is clear that the most important non-covalent interaction is the O…H contacts. No other contacts appeared as red spot in the d_{norm} which exclude the importance of these interactions in the molecular packing. The shortest O…H interactions are O2…H8B and O1…H2 contacts. Their interaction distances are 2.546 and 2.118 Å, respectively. Also, no evidences from the curvedness and shape index about the presence of π-π stacking interactions.

Presentation of all possible intermolecular interactions and their contributions in the molecular packing is shown in Fig. 9. The most dominant contacts are the H…H, Cl…H, O…H and C…H non-covalent interactions where their percentages are calculated to be 36.5, 19.5, 13.7 and 12.5%, respectively. In the same figure

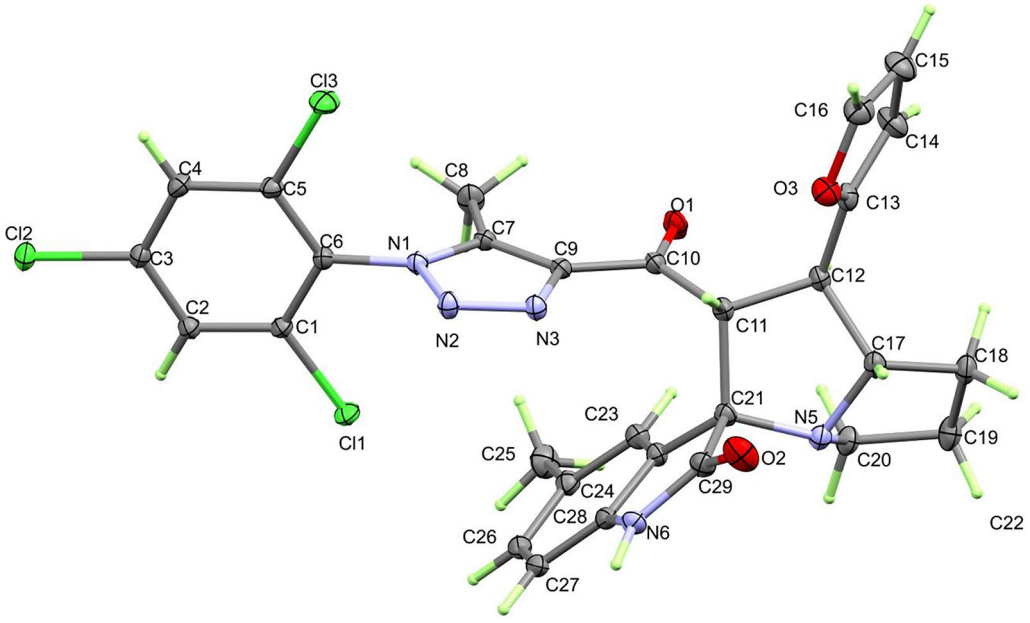

Fig. 3 X-ray structure of **4b**. The displacement ellipsoids are drawn at 50% probability level

the fingerprint of the O…H interactions is presented. It clearly seen as sharp spikes occurred at short distances which further revealed the importance of the O…H non-covalent interactions in the molecular packing of **4b**.

MEDT study of the 32CA reaction between AYs 5a, b and chalcones 1a, b

Analysis of the reactivity indices of the reagents

Analysis of quantum chemical reactivity indices [37–39] is a powerful tool to predict and understand the reactivity in cycloaddition reactions. The global reactivity indices, namely, the electronic chemical potential μ, chemical hardness η, electrophilicity ω, and nucleophilicity *N*, at the ground state of chalcones **1a**,**b** and the in situ generated AYs **5a**,**b** are gathered in Table 4.

The electronic chemical potentials [40] μ of AYs **5a**, –3.17 eV, and **5b**, –2.94 eV, are higher than those of chalcones **1a**,**b**, ca. –4.3 eV, indicating that along a polar 32CA reaction, the electron density will flux from the AYs to the chalcones. This behavior allows classifying these 32CA reactions as forward electron density flux (FEDF) processes [41, 42] in which the AYs are identified as the nucleophilic species and the chalcones as the electrophilic component.

The chemical hardness [40] η values of chalcones **1a**,**b**, ca. 7.6 eV, are higher than those of the AYs, ca. 6.9 eV, showing a higher tendency of the latter species to electron density deformation.

The electrophilicity [43] ω and nucleophilicity [44] *N* indices chalcones **1a**,**b** are ca. 1.2 and 3.3 eV, respectively, being classified as strong electrophiles and strong nucleophiles within the corresponding electrophilicity and nucleophilicity scales defined at the ωB97X-D/6-311G(d, p) computational level [45]. Consequently, these compounds can be categorized as ambiphilic species [46]. Substitution of the furan ring by the thiophene ring causes no significant changes in the reactivity of these α,β-unsaturated carbonyl compounds. Only the electrophilicity ω index increases very slightly, by 0.1 eV.

On the other hand, the electrophilicity ω indices of AYs **5a** and **5b** are 0.73 and 0.63 eV, respectively, which allow classifying these TACs as moderate electrophiles [45]. The nucleophilicity *N* indices, 4.79 (**5a**) and 5.01 (**5b**) eV, permit their classification as supernucleophilic species for being higher than 3.96 e [39, 45]. This behavior is typical of AYs [47], which are usually very reactive and unstable nucleophilic reagents that need to be generated in situ. Substitution of one H atom at AY **9** by the electron-withdrawing chlorine –Cl atom decreases the nucleophilicity *N* index of AY **5a** by 0.18 eV, while substitution by electron-donating –Me group scarcely enhances the nucleophilicity of AY **5b** by only 0.04 eV. Thus, substitution at AY **9** neither causes significant changes in the reactivity of these TACs.

The supernucleophilic character of AY **5a**,**b** together with the strong electrophilic character of chalcones **1a**,**b** suggest that the corresponding 32CA reactions of FEDF will have a high polar character. The high polar character facilitates the reaction through more favorable nucleophilic/electrophilic interactions that will lead to lower activation energies.

Along a polar reaction involving non-symmetric species, the most favorable reaction path is that involving the two-center interaction between the most nucleophilic

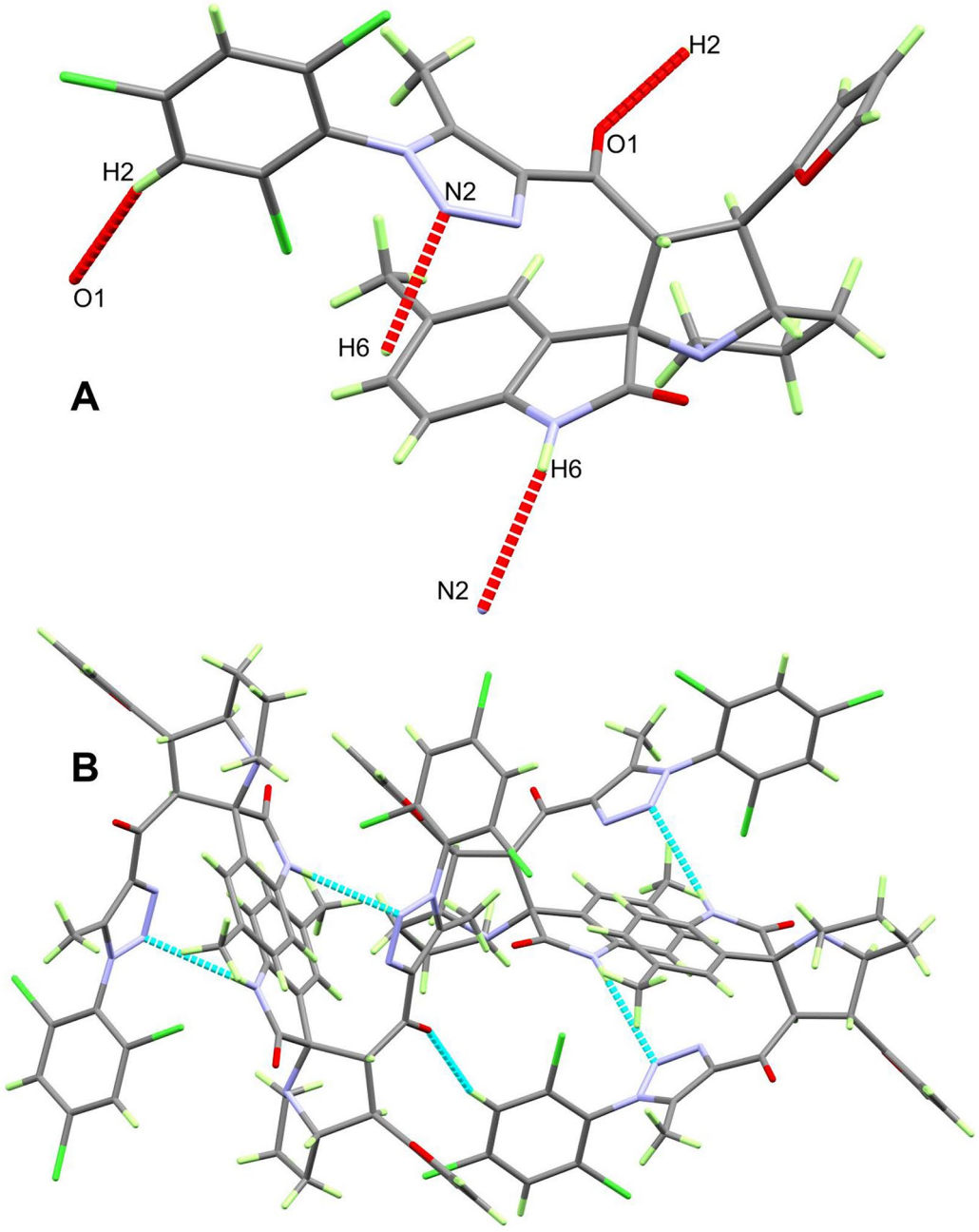

Fig. 4 The important contacts (**A**) and H-bond scheme (**B**) for **4b**

and the most electrophilic centers of the two reagents [48]. The analysis of the nucleophilic P_k^- and electrophilic P_k^+ Parr functions [49] has shown to be an accurate tool for the study of the local reactivity in polar processes. Hence, according to the global reactivity of the reagents, the nucleophilic P_k^- Parr functions of AY **5a** and the electrophilic P_k^+ Parr functions of the more electrophilic chalcone **1a** were analyzed (see Fig. 10).

Analysis of the nucleophilic P_k^- Parr functions of AY **5b** indicates that the C1 carbon, P_{C1}^- = 0.44, is slightly more nucleophilically activated than the C3 carbon, P_{C3}^- = 0.30 (see Scheme 2 for atom labels). Note that similar AYs have been previously characterized [50, 51] to present a reactive *pseudoradical* center [52] at the more nucleophilic C1 carbon, classifying these species as *pseudo(mono)radical* TACs [29]. On the other hand, analysis of the electrophilic P_k^+ Parr functions of chalcone **1a** shows that the β-conjugated C4 carbon, P_{C4}^+ = 0.30, is considerably more electrophilic than the carbonyl C6 carbon, P_{C6}^+ = 0.19. Consequently, according to the local nucleophilic and electrophilic properties, the most favorable two-center interaction along the 32CA reaction of

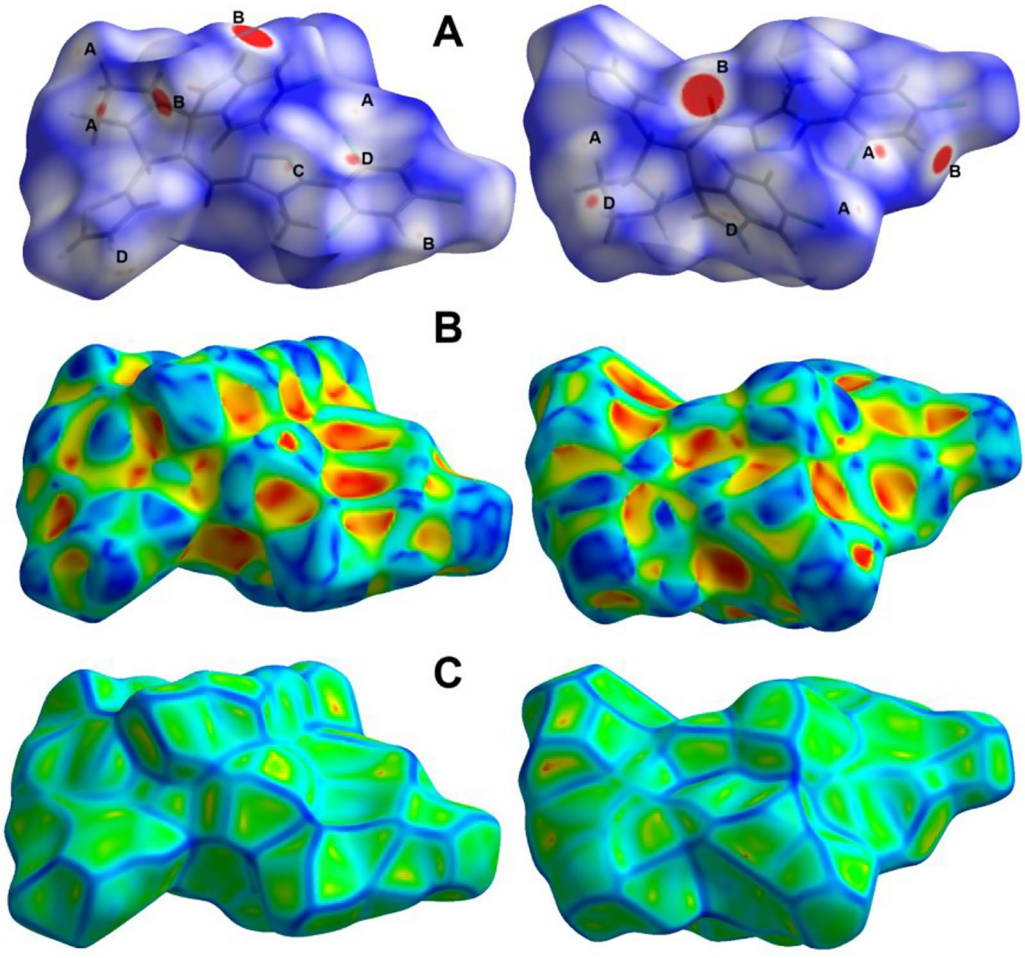

Fig. 5 Hirshfeld d_{norm}, shape index and curvedness maps for **4a** showing the most important interactions; A) Cl…H, B) O…H, C) N…H and D) C…H

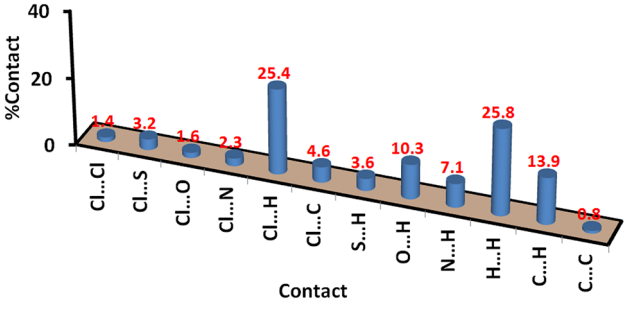

Fig. 6 Intermolecular contacts and their percentages in **4a**

AYs **5a**,**b** with chalcones **1a**,**b** should take place between the C1 and C4 carbon atoms, leading to the *meta* regioisomeric cycloadducts (see later, Scheme 2).

Study of the competitive reaction paths

Due to the non-symmetry of the reagents, the 32CA reaction between AYs **5a**,**b** and chalcones **1a**,**b** can take place along two *ortho/meta* regioisomeric reaction paths and two *endo/exo* stereoisomeric approach modes, leading to a total of four competitive pathways (see Scheme 2). Considering that the β-conjugated C4 carbon of chalcones **1a**,**b** is the most electrophilic center, only the chemoisomeric reaction path involving the C4–C5 double bond has been computationally studied herein. Note, indeed, that the corresponding chemoisomeric reaction paths on the C6–O7 carbonyl bond of similar chalcones have been ruled out in analogous 32CA reactions [36]. Furthermore, the potential energy surface is explored only for the 32CA reaction involving the most electrophilic reagent, i.e. chalcone **1a** with AY **5a**. A conformational analysis of the reagents and products was performed whenever different conformers were possible in order to consider only the most stable structures. The enthalpy profiles associated with the four competitive reaction paths are represented in Fig. 11, while full thermodynamic data are given in Table S2 in the Supplementary Material.

Analysis of the stationary points found along the four considered reaction paths indicates that the 32CA reaction between AY **5a** and chalcone **1a** takes place through a one-step mechanism. Each reaction path starts with the formation of a stable molecular complex (MC) by weak intermolecular interactions between the reagents.

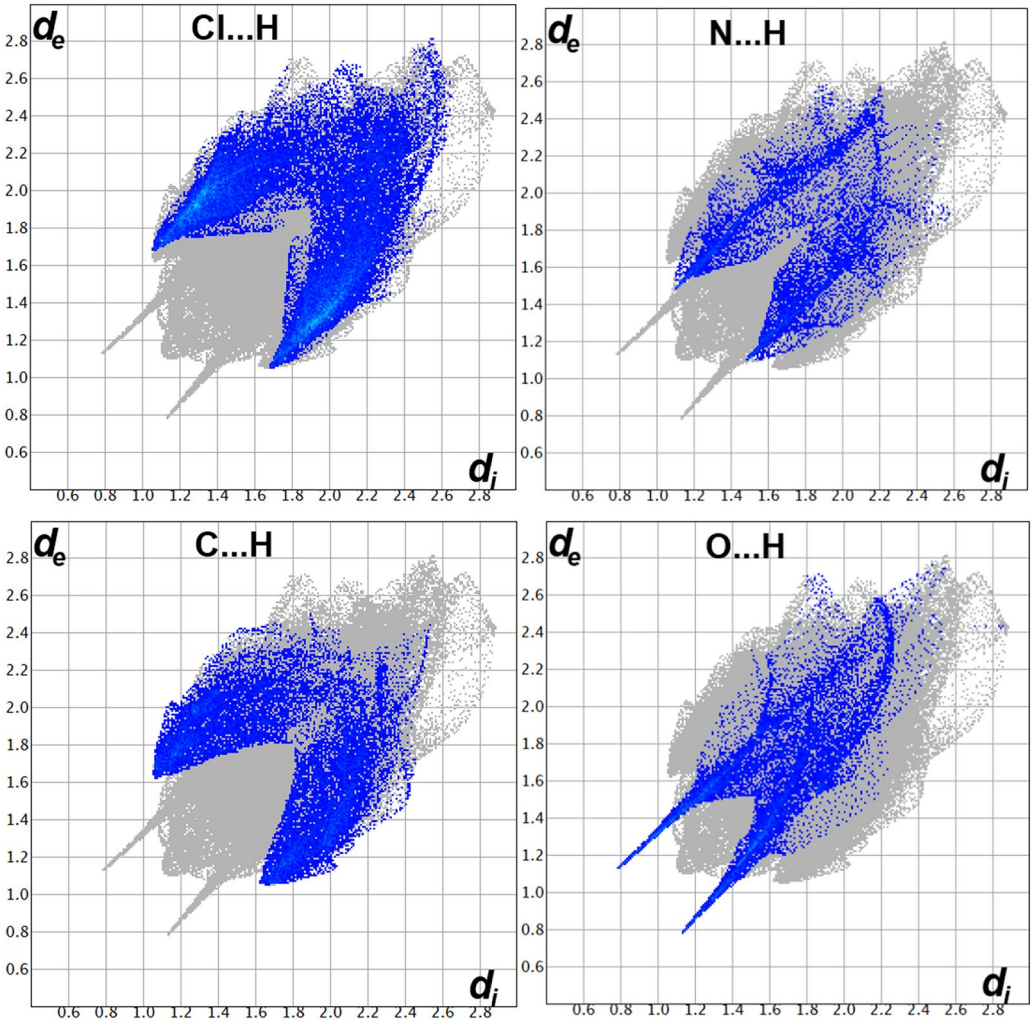

Fig. 7 Decomposed fingerprint plots for the short contacts in **4a**

Table 3 Interaction distances for the short contacts in **4a**

Contact	Distance	Contact	Distance
O2…H**4a**	2.248	Cl3…H22A	2.816
O1…H4	1.912	C14…H27	2.745
O1…H2	2.565	C15…H27	2.734
Cl4…H21B	2.759	C6…H21A	2.691
Cl3…H23	2.738	N2…H28	2.59

However, due to the thermodynamic equilibrium between the several MCs, only the most stable complex, **MC-on**, was selected as the energy reference. Formation of **MC-on** is strongly exothermic by 16.9 kcal·mol^{-1} (see Scheme 2 and Fig. 11). Considering the formation of **MC-on**, the activation enthalpies for the four isomeric paths range from 12.0 kcal·mol^{-1} (**TS-on**) to 16.3 kcal·mol^{-1} (**TS-mx**). On the other hand, the reaction enthalpies are found between –36.0 (**6a**) and –39.6 (**4a**) kcal·mol^{-1}. The highly exothermic character of this reaction suggests that the 32CA reactions is irreversible under the experimental conditions. Together with the relatively short reaction time (5 h), a kinetic control of the product mixture is expected. As the *meta* **TS-mn** and *exo***TS-ox** are 1.0 and 3.2 kcal·mol^{-1} higher in energy than the more favourable **TS-on**, a high *ortho* regioselectivity and a total *endo* stereoselectivity is computationally obtained, which accounts for the exclusive experimental formation of **4a** via **TS-on**.

Both the experimental and computational regioselectivity differ from the *meta* regioselectivity predicted by analysis of the Parr functions. This is because there can be other factors that overcome the weight of the local nucleophilic/electrophilic interactions, such as non-covalent interactions. Indeed, a previous theoretical study of a similar 32CA reaction [50] revealed that the formation of two intermolecular hydrogen bonds between the two interacting frameworks at the most favorable **TS-on** accounted for the unexpected *ortho* regioselectivity experimentally observed.

The optimized geometries of the four isomeric transition states (TSs) in methanol are represented in Fig. 12.

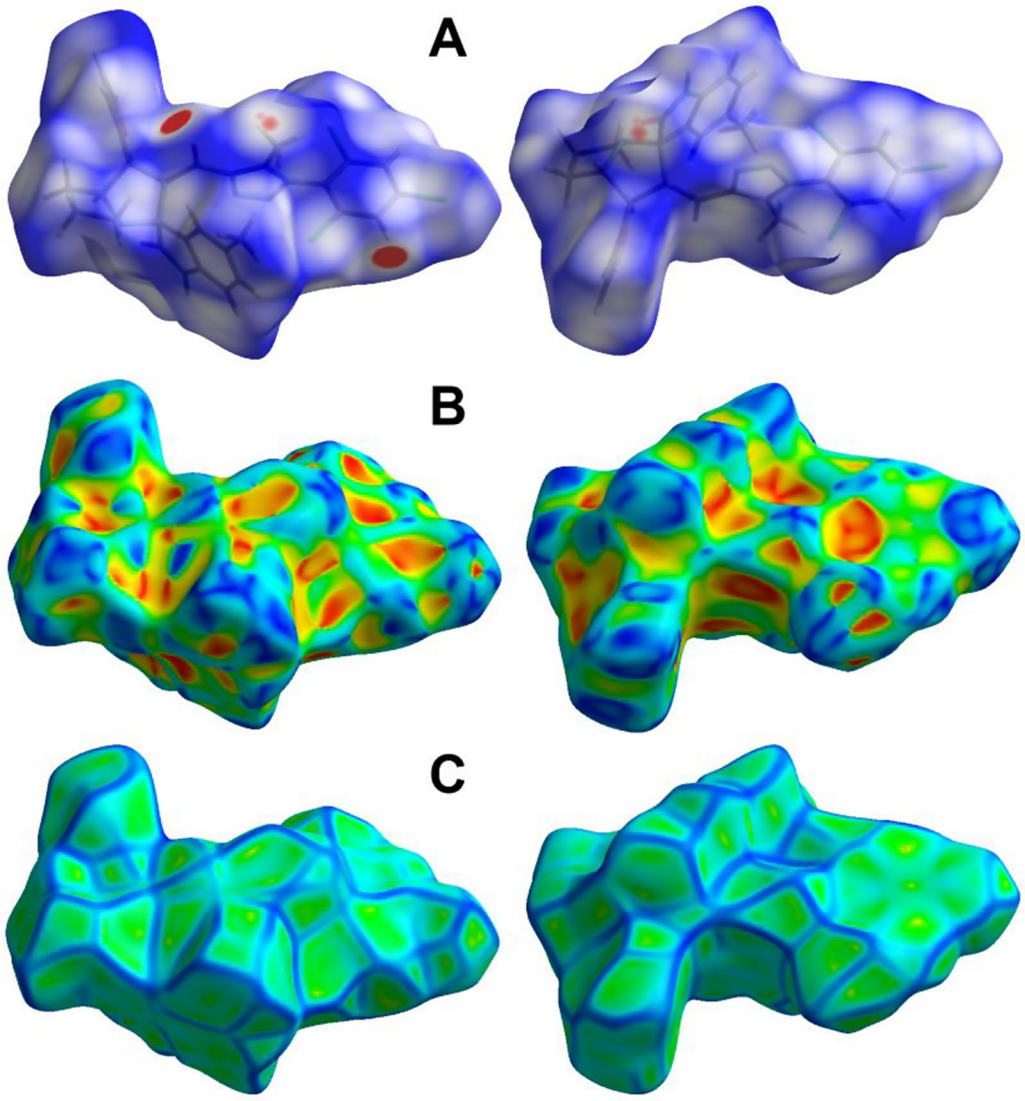

Fig. 8 Hirshfeld d_{norm}, shape index and curvedness maps for **4b** showing the most important interactions as intense red spots

The C–C distances between the interacting carbons provide insights into the new single-bond formation processes. Except for the most unfavorable **TS-mx**, the other three TSs exhibit an asynchronous behavior, with the shorter C–C distance involving the most electrophilic β-conjugated C4 carbon of chalcone **1a**. The most favorable **TS-on**, characterized by C3–C4 and C1–C5 distances of 2.085 and 2.703 Å, respectively, has the highest degree of asynchronicity. Examining the intrinsic reaction coordinate (IRC) path [53] from the highly asynchronous **TS-on** to **4a** reveals that the 32CA reaction follows a non-concerted *two-stage,one-step* mechanism [46]. In this mechanism, the formation of the second C1–C5 single bond begins only after the first C3–C4 single bond is fully formed.

Finally, analysis of the global electron density transfer (GEDT) [54] at the most favorable **TS-on** allows quantifying the polar behavior of this 32CA reaction. GEDT values lower than 0.05 e correspond to non-polar processes, while values higher than 0.20 e characterize polar processes. The GEDT values at the four TSs are given in Fig. 12. The GEDT at **TS-on** is 0.29 e. This high value, which is the result of the supernucleophilic character of AY **5a** and the strong electrophilic characteristic of chalcone **1a** (see Table 4), confirms the high polar nature of this 32CA reaction, which accounts for its low activation enthalpy of 12.0 kcal·mol^{-1} via **TS-on** and the complete *endo* stereoselectivity. Note that polar cycloaddition reactions normally exhibit *endo* stereoselectivity. The direction of the flux of the electron density, from AY **5a** to chalcone **1a**, allows classifying this 32CA reaction as FEDF [41, 42], in agreement with the analysis of the reactivity indicators.

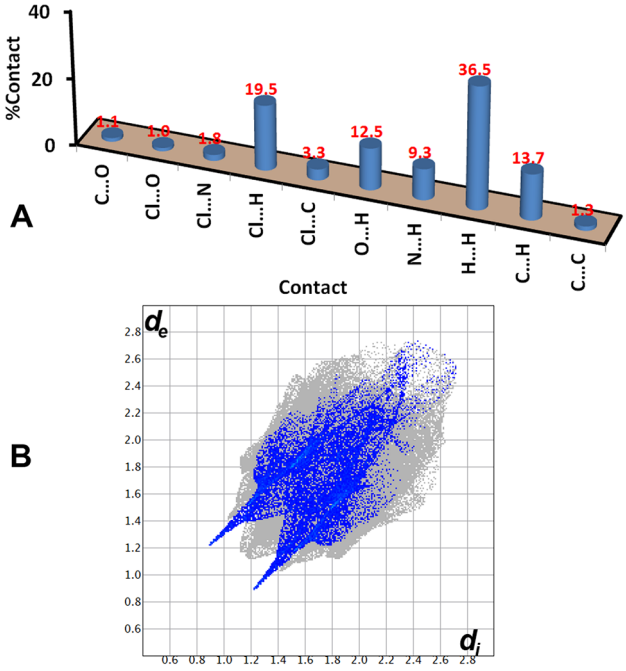

Fig. 9 Intermolecular contacts and their percentages (**A**) and the fingerprint plot for the short O…H contacts (**B**) in **4b**

Table 4 ωB97X-D/6-311G(d, p) gas-phase electronic chemical potential μ, chemical hardness η, electrophilicity ω, and nucleophilicity *N*, at the ground state of chalcones **1a**,**b** and AYs **5a**,**b**. data for the unsubstituted AY **9** is also included

	μ	η	ω	*N*
Chalcone **1a** (–S)	−4.33	7.63	1.23	3.26
Chalcone **1b** (–O)	−4.21	7.61	1.16	3.38
AY **5a** (–Cl)	−3.17	6.87	0.73	4.79
AY **9** (–H)	−2.97	6.90	0.64	4.97
AY **5b** (–Me)	−2.94	6.89	0.63	5.01

Materials and methods

Synthesis of 1-(5-methyl-1-(2,4,6-trichlorophenyl)-1 H-1,2,3-triazol-4-yl)ethan-1-one 1

To a stirring solution of 2,4,6-trichloroaniline (6.05 g, 0.0308 mol) in dil. HCl (40 mL, 3 M). A solution of sodium nitrite (2.34 g, 0.0339 mol, 25 mL, 1 M) is treated at temperature < 10 °C. The progress of the reaction is confirmed by liberation of brown gases (1 h). When the brown gases crases a solution of sodium azide (4.006 g, 0.0616 mol) is added to the stirring cold reaction mass. The formation of product is confirmed by TLC (1 h). The reaction mixture was extracted using diethylether. A brown viscous liquid confirmed the product **1**.

A solution of the appropriate azide (10.0 mmol, 2.22 gm) and acetylacetone (2.0 g, 20.0 mmol) in $CHCl_3$ (20 ml) was treated by adding Et_3N (2.02 g, 20.0 mmol) and DBU (0.76 g, 5.00 mmol). The reaction mixture was stirred at room temperature for 1–2 h. The solvent was removed and water is added then extracted with Et_2O, dried with Na_2SO_4, evaporated and the solid product was washed with the n-hexane to provide pure compound.

^{1}H NMR (500 MHz, DMSO-d_6) δ 8.14 (s, 2 H), 2.66 (s, 3 H), 2.68–2.62 (m, 1H), 2.37 (s, 3 H); ^{13}C NMR (126 MHz, DMSO-d_6) δ 193.55, 142.99, 140.00, 138.09, 134.38, 130.07, 129.66, 28.15, 8.99. m.p: 131 °C; powder.

Synthesis of the chalcones 2a, b

(E)-1-(5-Methyl-1-(2,4,6-trichlorophenyl)-1 H-1,2,3-triazol-4-yl)-3-(thiophen-2-yl)prop-2-en-1-one 2a

A mixture of thiophene-2-carbaldehyde (2 mmol, 224 mg) and 1-(5-methyl-1-(2,4,6-trichlorophenyl)-1*H*-1,2,3-triazol-4-yl)ethan-1-one **1** (0.609 g, 2.0 mmol) dissolved in ethanol (20 mL) was added slowly to an aqueous solution of potassium hydroxide (2.0 mmol, 112 mg) in water (10 mL). The mixture was stirred in crushed-ice bath for 2 h, stirred at 20 ~ 25 ℃ for 4 h. The mixture was filtrated and the residue was washed with cold water and cold alcohol dried to give the titled compound without further purification.

m.p: 327 °C; powder. ^{1}H NMR (400 MHz, $CDCl_3$) δ 8.07 (d, *J* = 15.8 Hz, 1H), 7.86 (d, *J* = 15.4 Hz, 1H), 7.57 (s, 2 H), 7.43 (dd, *J* = 11.8, 4.4 Hz, 2 H), 7.13–7.05 (m, 1H), 2.49 (s, 2 H), 2.51–2.39 (m, 1H); ^{13}C NMR (101 MHz, $CDCl_3$) δ 183.80, 143.45, 140.61, 140.54, 138.16, 136.61, 135.13, 132.37, 130.06, 129.45, 129.25, 129.16, 128.36, 121.82, 9.29.

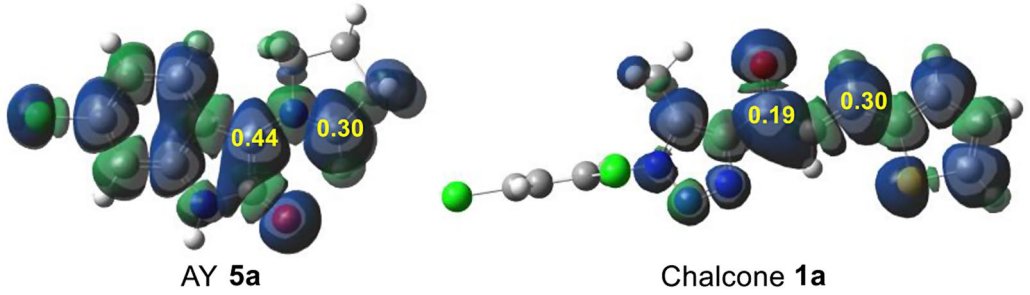

Fig. 10 ωB97X-D/6-311G(d, p) gas-phase nucleophilic P_k^- Parr functions of AY **5a** and most relevant electrophilic P_k^+ Parr functions of the more electrophilic chalcone **1a**

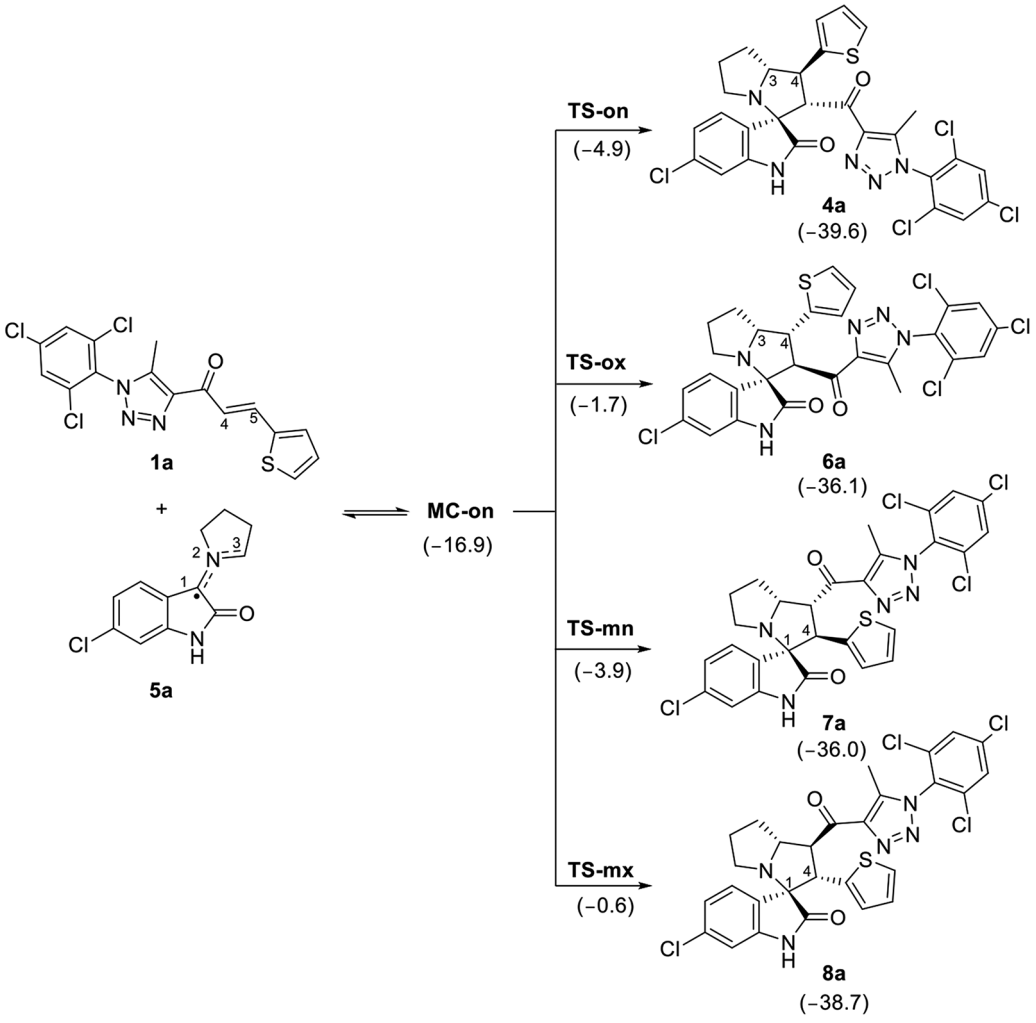

Scheme 2 Studied competitive reaction paths associated with the 32CA reaction of AY **5a** with chalcone **1a**. ωB97X-D/6-311G(d, p) relative enthalpies, in methanol, are given in kcal·mol^{-1}

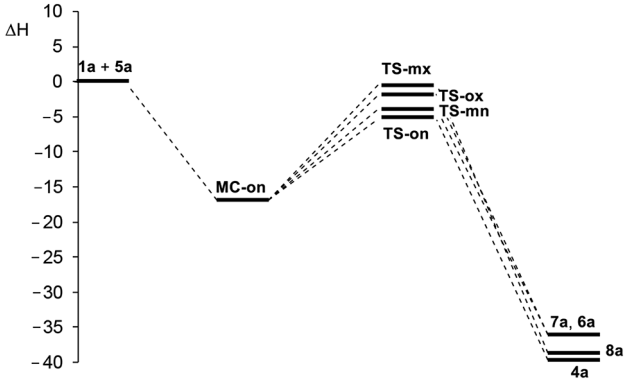

Fig. 11 ωB97X-D/6-311G(d, p) enthalpy profile, in methanol, for the 32CA reaction of AY **5a** with chalcone **1a**. Enthalpies are given in kcal·mol^{-1}

(E)-3-(Furan-2-yl)-1-(5-methyl-1-(2,4,6-trichlorophenyl)-1 H-1,2,3-triazol-4-yl)prop-2-en-1-one 2b

A mixture of furan-2-carbaldehyde (2 mmol, 192 mg) and 1-(5-methyl-1-(2,4,6-trichlorophenyl)-1*H*-1,2,3-triazol-4-yl)ethan-1-one **1** (0.609 g, 2.0 mmol) dissolved in ethanol (20 mL) was added slowly to an aqueous solution of potassium hydroxide (2.0 mmol, 112 mg) in water (10 mL). The mixture was stirred in crushed-ice bath for 2 h, stirred at 20 ~ 25 ℃ for 4 h. The mixture was filtrated and the residue was washed with cold water and cold alcohol dried to give the titled compound without further purification.

m.p: 80 °C; powder. ^{1}H NMR (400 MHz, $CDCl_3$) δ 7.92 (d, *J* = 15.5 Hz, 1H), 7.71 (d, *J* = 15.9 Hz, 1H), 7.55 (d, *J* = 11.8 Hz, 3 H), 6.77 (d, *J* = 3.5 Hz, 1H), 6.50 (d, *J* = 2.9 Hz, 1H), 2.49 (s, 3 H); ^{13}C NMR (101 MHz, $CDCl_3$) δ 184.02, 151.90, 145.23, 143.51, 140.46, 138.13, 135.13, 130.48, 130.08, 129.12, 121.29, 116.75, 112.52, 9.40.

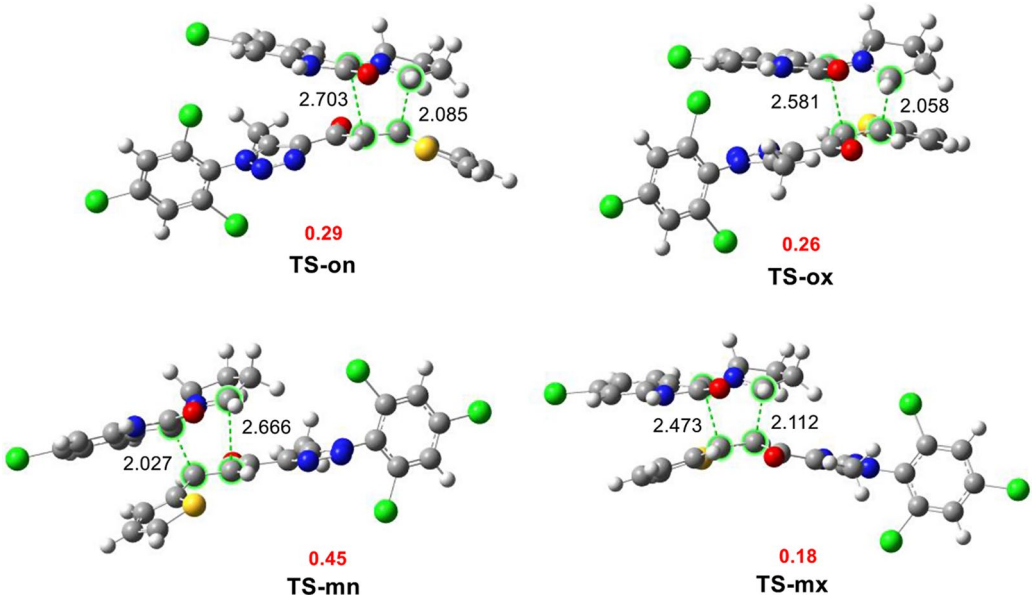

Fig. 12 ωB97X-D/6-311G (d, p) optimized geometries in methanol of the TSs involved in the 32CA reaction of AY **5a** with chalcone **1a**. Distances are expressed in angstroms, Å, while GEDT values, in red, are given in average number of electrons, e

Synthesis of spirooxindoles derviatives 4a, b

(1′S,2′S,3R)-6-Chloro-2′-(5-methyl-1-(2,4,6-trichlorophenyl)-1 H-1,2,3-triazole-4-carbonyl)-1′-(thiophen-2-yl)-1′,2′,5′,6′,7′,7a′-hexahydrospiro[indoline-3,3′-pyrrolizin]-2-one 4a

A mixture of **2a** (198.5 mg, 0.5mmol), 6-Cl- isatin (90.5 mg, 0.5 mmol) and L-proline (57.5 mg, 0.5 mmol) in methanol (10 mL) was refluxed on oil bath for appropriate time 5–8 h. After completion of the reaction as evident from TLC, the reaction was kept at room temperature overnight and the solid precipitated was filtered off without any further purification as faint yellow crystalline compound. As an example, the reaction has been scaled up to a 1-mole scale, and it remains producible without affecting the chemical structure or the chemical yield.

m.p: 161 °C; crystal. ^{1}H NMR (500 MHz, DMSO-d_6) δ 10.28 (s, 1H), 7.99 (s, 1H), 8.04–7.94 (m, 1H), 7.32 (dd, *J*=5.1, 1.2 Hz, 1H), 6.98 (dt, *J*=3.2, 1.1 Hz, 1H), 6.95–6.80 (m, 2 H), 6.48 (dd, *J*=8.4, 4.5 Hz, 1H), 4.86 (d, *J*=10.8 Hz, 1H), 4.15–3.99 (m, 2 H), 3.25 (d, *J*=7.6 Hz, 2 H), 3.22 (s, 1H), 2.75 (td, *J*=8.8, 6.4 Hz, 1H), 2.36 (s, 1H), 2.43–2.28 (m, 1H), 1.97–1.83 (m, 2 H), 1.79–1.61 (m, 1H), 1.71 (s, 1H); ^{13}C NMR (126 MHz, DMSO-d_6) δ 191.45, 178.74, 157.69, 155.81, 142.84, 141.77, 139.40, 138.61, 137.26, 133.68, 133.28, 129.11, 129.08, 128.50, 126.85, 124.47, 124.07, 115.46, 115.28, 114.17, 113.97, 109.88, 71.48, 70.40, 65.62, 47.64, 45.27, 27.77, 25.37, 7.46.

(1′S,2′S,3R)-1′-(Furan-2-yl)-5-methyl-2′-(5-methyl-1-(2,4,6-trichlorophenyl)-1 H-1,2,3-triazole-4-carbonyl)-1′,2′,5′,6′,7′,7a′-hexahydrospiro[indoline-3,3′-pyrrolizin]-2-one 4b

A mixture of **2b** (190.5 mg, 0.5mmol), 5-Me- isatin (80.5 mg, 0.5 mmol) and L-proline (57 0.5 mg, 0.5 mmol) in methanol (10 mL) was refluxed on oil bath for appropriate time 5–8 h. After completion of the reaction as evident from TLC, the reaction was kept at room temperature overnight and the solid precipitated was filtered off without any further purification as faint yellow crystalline compound.

m.p: 193 °C; crystal. ^{1}H NMR (400 MHz, DMSO-d_6) δ 10.23 (s, 1H), 8.09–8.00 (m, 2 H), 7.59 (s, 1H), 6.82 (d, *J*=7.3 Hz, 2 H), 6.48–6.37 (m, 2 H), 6.27 (d, *J*=3.5 Hz, 1H), 4.99 (d, *J*=10.7 Hz, 1H), 4.14 (ddd, *J*=10.7, 7.0, 3.8 Hz, 1H), 3.97 (t, *J*=10.4 Hz, 1H), 3.33 (d, *J*=7.3 Hz, 1H), 2.85 (q, *J*=8.4 Hz, 1H), 2.49–2.27 (m, 2 H), 2.14 (s, 3 H), 1.99 (s, 3 H), 2.12–1.63 (m, 4 H); ^{13}C NMR (126 MHz, DMSO-d_6) δ 192.68, 179.58, 154.37, 142.67, 140.81, 140.08, 138.02, 134.69, 134.10, 129.43, 127.89, 125.56, 110.98, 109.71, 106.30, 71.77, 67.98, 62.36, 48.62, 44.28, 28.56, 25.73, 21.05, 8.29.

X-Ray structure determination

Crystals **4a** and **4b** were immersed in cryo-oil, mounted in a loop, and measured at a temperature of 120 K. "The X-ray diffraction data were collected on a Rigaku Oxford Diffraction Supernova diffractometer using Mo Kα radiation. The *CrysAlisPro* [55] software package was used for cell refinements and data reductions. A multi-scan (**4a**) or an analytical (**4b**) absorption correction (*CrysAlisPro*) [55] was applied to the intensities before the structure

solution. The structures were solved by the intrinsic phasing (*SHELXT*) [56] method. Structural refinements were carried out using *SHELXL* [57] software with *SHELXLE* [58] graphical user interface. The NH hydrogen atoms, involved in hydrogen bonding, were located from the difference Fourier map and refined isotropically. All other hydrogen atoms were positioned geometrically and constrained to ride on their parent atoms, with C-H=0.95-1.00 Å and U_{iso} = 1.2–1.5·U_{eq}(parent atom). The crystallographic details are summarized in Table 1. The topology analyses were performed using Crystal Explorer 17.5 program [59]".

Conclusions

By Employing the 32CA approach two new spirooxindoles analoges successfully synthesized incorporated a triazole unit with thiophene and/or furan motif scaffold. Hirshfeld analysis based on the experimental X-ray structure, the molecular and supramolecular structures of both organic hybrids were described. The twist of the aryl and the triazole moieties is less (84.75˚) for **4a** than that for **4b** (86.64˚). The supramolecular structure of **4a** is controlled by the Cl…H, O…H, N…H and C…H non-covalent interactions while in **4b** the O…H interactions are the most important. By Employing the 32CA approach two new spirooxindoles analoges successfully synthesized incorporated a triazole unit with thiophene and/or furan motif scaffold. Hirshfeld analysis based on the experimental X-ray structure, the molecular and supramolecular structures of both organic hybrids were described. The twist of the aryl and the triazole moieties is less (84.75˚) for **4a** than that for **4b** (86.64˚). The supramolecular structure of **4a** is controlled by the Cl…H, O…H, N…H and C…H non-covalent interactions while in **4b** the O…H interactions are the most important.

The MEDT study of the key 32CA reaction step reveals that the low activation energies and high experimental selectivity are the result of the supernucleophilic character of the in situ generated azomethine ylides and the strong electrophilicity of the chalcones, which favour the process through a high polar character. This high polar character accounts for the total *endo* selectivity experimentally found.

Supplementary Information

The online version contains supplementary material available at https://doi.org/10.1186/s13065-024-01343-8.

Supplementary Material 1: The online version contains supplementary material available at xxxx, Figure S1-S10: NMR spectrum; Computational Protocol; Table S1. Bond lengths (Å) and angles (°) for 4a and 4b. Table S2. ωB97X-D/6-311G(d, p) enthalpies, entropies, and Gibbs free energies, and the relative ones with respect to the separated reagents, for the stationary points involved in the 32CA reaction of AY 5a with chalcone 1a.; Cartesian coordinates and electronic energies of the stationary points involved in the 32CA reaction between AY 5a and chalcone 1a in methanol. Imaginary frequencies for TSs at 65 ºC are included.

Acknowledgements

The author would like to extend their sincere appreciation to the Researchers Supporting Project (RSP2024R64), King Saud University, Riyadh, Saudi Arabia. This work has also been supported by the Ministry of Science and Innovation (MICINN) of the Spanish Government, through the project PID2019-110776GB-I00 (AEI/FEDER, UE).

Author contributions

Conceptualization, A.B.; methodology, M.A., M.A.A., M.K.A.-M., A.A.A., M.R.-G.; software, S.M.S., M.H., M.R.-G.; validation, S.M.S. and A.M.A.-M.; formal analysis, M.A., M.A.A., M.H., M.K.A.-M., A.A.A.; investigation, M.A., M.A.A., M.K.A.-M., A.A.A, M.R.-G.; resources, A.B.; data curation, S.M.S.; writing—original draft preparation, S.M.S., M.R.-G., and A.B.; writing—review and editing, All; supervision, A.A.A.; M.K.A.-M., and A.B.; funding acquisition, M.A. All authors have read and agreed to the published version of the manuscript.

Data availability

The datasets that are not included in this article can be shared with the corresponding author upon request. "The x-ray crystal datasets generated and/or ana-lysed during the current study are available in the Cambridge Structural Database repository, https://www.ccdc.cam.ac.uk/structures/ and access number to datasets: 2303110 for 4a and 2303111 for compound 4b].

Declarations

Ethics approval and consent to participate

Not applicable.

Consent for publication

Not applicable.

Competing interests

The authors declare no competing interests.

Received: 26 January 2024 / Accepted: 1 November 2024
Published online: 14 November 2024

References

1. Cerulli V, Banfi L, Basso A, Rocca V, Riva R. Diversity oriented and chemoenzymatic synthesis of densely functionalized pyrrolidines through a highly diastereoselective ugi multicomponent reaction. Org Biomol Chem. 2012;10(6):1255.
2. Ganem B. Strategies for innovation in multicomponent reaction design. Acc Chem Res. 2009;42(3):463–72.
3. Dömling A. Recent developments in Isocyanide based multicomponent reactions in Applied Chemistry. Chem Rev. 2005;106(1):17–89.
4. Toumi A, Abdella FI, Boudriga S, Alanazi TY, Alshamari AK, Alrashdi AA, Dbeibia A, Hamden K, Daoud I, Knorr M. Synthesis of Tetracyclic Spirooxindolepyrrolidine-Engrafted Hydantoin scaffolds: Crystallographic Analysis, Molecular Docking studies and evaluation of their Antimicrobial, anti-inflammatory and analgesic activities. Molecules. 2023;28(21):7443.
5. Toumi A, Boudriga S, Mandour YM, Mekki AA, Knorr M, Strohmann C, Kirchhoff J-L, Sobeh M. Design of Novel Enantiopure Dispirooxindolopyrrolidine-Piperidones as Promising candidates toward COVID-19: asymmetric synthesis, Crystal structure and in Silico studies. Molecules. 2022;27(12):3945.
6. Hammouda MB, Boudriga S, Hamden K, Askri M, Knorr M, Strohmann C, Brieger L, Krupp A, Snoussi M, Aouadi K. New spiropyrrolothiazole derivatives bearing an oxazolone moiety as potential antidiabetic agent: design, synthesis, crystal structure, Hirshfeld surface analysis, ADME and molecular docking studies. J Mol Struct. 2022;1254:132398.
7. Jossang A, Jossang P, Hadi HA, Sevenet T, Bodo B. Horsfiline, an oxindole alkaloid from Horsfieldia superba. J Org Chem. 1991;56(23):6527–30.
8. Cui C-B, Kakeya H, Osada H. Novel mammalian cell cycle inhibitors, spirotryprostatins A and B, produced by aspergillus fumigatus, which inhibit mammalian cell cycle at G2/M phase. Tetrahedron. 1996;52(39):12651–66.

9. García Prado E, García Gimenez MD, De la Puerta Vázquez R, Espartero Sánchez JL. Sáenz Rodríguez MT: antiproliferative effects of mitraphylline, a pentacyclic oxindole alkaloid of Uncaria tomentosa on human glioma and neuroblastoma cell lines. Phytomedicine. 2007;14(4):280–4.
10. Al-Majid AM, Ali M, Islam MS, Alshahrani S, Alamary AS, Yousuf S, Choudhary MI, Barakat A. Stereoselective synthesis of the Di-Spirooxindole Analogs Based Oxindole and Cyclohexanone Moieties as potential Anticancer agents. Molecules. 2021;26(20):6305.
11. Barakat A, Islam MS, Ali M, Al-Majid AM, Alshahrani S, Alamary AS, Yousuf S, Choudhary MI. Regio- and Stereoselective Synthesis of a New Series of Spirooxindole Pyrrolidine Grafted Thiochromene scaffolds as potential Anticancer agents. Symmetry. 2021;13(8):1426.
12. Kornet MJ, Thio AP. Oxindole-3-spiropyrrolidines and -piperidines. Synthesis and local anesthetic activity. J Med Chem. 1976;19(7):892–8.
13. Rajanarendar E, Ramakrishna S, Govardhan Reddy K, Nagaraju D, Reddy YN. A facile synthesis, anti-inflammatory and analgesic activity of isoxazolyl-2,3-dihydrospiro[benzo[f]isoindole-1,3′-indoline]-2′,4,9-triones. Bioorg Med Chem Lett. 2013;23(13):3954–8.
14. Rajesh SM, Perumal S, Menéndez JC, Yogeeswari P, Sriram D. Antimycobacterial activity of spirooxindolo-pyrrolidine, pyrrolizine and pyrrolothiazole hybrids obtained by a three-component regio- and stereoselective 1,3-dipolar cycloaddition. MedChemComm. 2011;2(7):626.
15. Bhaskar G, Arun Y, Balachandran C, Saikumar C, Perumal PT. Synthesis of novel spirooxindole derivatives by one pot multicomponent reaction and their antimicrobial activity. Eur J Med Chem. 2012;51:79–91.
16. Altowyan MS, Barakat A, Al-Majid AM, Al-Ghulikah HA. Spiroindolone Analogues as potential hypoglycemic with dual inhibitory activity on α-Amylase and α-Glucosidase. Molecules. 2019;24(12):2342.
17. Zhou W-H, Xu X-G, Li J, Min X, Yao J-Z, Dong G-Q, Zhuang C-L, Miao Z-Y, Zhang W-N. Design, synthesis and structure–activity relationship of 4,5-dihydropyrrolo[3,4- c]pyrazol-6(1 H)-ones as potent p53-MDM2 inhibitors. Chin Chem Lett. 2017;28(2):422–5.
18. Barakat A, Alshahrani S, Mohammed Al-Majid A, Saleh Alamary A, Haukka M, Abu-Serie MM, Dömling A, Mazyed EA, Badria FA, El-Senduny FF. Novel spirooxindole based benzimidazole scaffold: in vitro, nanoformulation and in vivo studies on anticancer and antimetastatic activity of breast adenocarcinoma. Bioorg Chem. 2022;129:106124.
19. Arumugam N, Almansour AI, Kumar RS, Dege N. A facile ionic liquid-accelerated, four-component cascade reaction protocol for the regioselective synthesis of biologically interesting ferrocene engrafted spiropyrrolidine hybrid heterocycles. J King Saud Univ - Sci. 2020;32(4):2500–4.
20. Zhou L-M, Qu R-Y, Yang G-F. An overview of spirooxindole as a promising scaffold for novel drug discovery. Expert Opin Drug Discov. 2020;15(5):603–25.
21. Barakat A, Alshahrani S, Al-Majid AM, Ali M, Altowyan MS, Islam MS, Alamary AS, Ashraf S, Ul-Haq Z. Synthesis of a new class of Spirooxindole-Benzo[b] Thiophene-Based molecules as acetylcholinesterase inhibitors. Molecules. 2020;25(20):4671.
22. Lotfy G, Abdel Aziz YM, Said MM, El Ashry ESH, El Tamany ESH, Abu-Serie MM, Teleb M, Dömling A, Barakat A. Molecular hybridization design and synthesis of novel spirooxindole-based MDM2 inhibitors endowed with BCL2 signaling attenuation; a step towards the next generation p53 activators. Bioorg Chem. 2021;117:105427.
23. Salmon AJ, Williams ML, Wu QK, Morizzi J, Gregg D, Charman SA, Vullo D, Supuran CT, Poulsen S-A. Metallocene-based inhibitors of Cancer-Associated Carbonic anhydrase enzymes IX and XII. J Med Chem. 2012;55(11):5506–17.
24. Al-Rasheed HH, Al-Majid AM, Ali M, Haukka M, Ramadan S, Soliman SM, El-Faham A, Domingo LR, Barakat A. [3 + 2] cycloadditions in asymmetric synthesis of spirooxindole hybrids linked to Triazole and Ferrocene Units: X-ray crystal structure and MEDT Study of the reaction mechanism. Symmetry. 2022;14(10):2071.
25. Kumar K, Carrère-Kremer S, Kremer L, Guérardel Y, Biot C, Kumar V. 1 < i > H-1,2,3-Triazole-Tethered isatin–ferrocene and isatin–ferrocenylchalcone conjugates: synthesis and in Vitro Antitubercular evaluation. Organometallics. 2013;32(20):5713–9.
26. Kumar K, Carrère-Kremer S, Kremer L, Guérardel Y, Biot C, Kumar V. Azide–alkynecycloadditionen route towards 1H-1,2,3-triazole-tethered β-lactam–ferrocene and β-lactam–ferrocenylchalcone conjugates: synthesis and in vitro anti-tubercular evaluation. Dalton Trans. 2013;42(5):1492–500.
27. Kumar K, Pradines B, Madamet M, Amalvict R, Benoit N, Kumar V. 1H-1,2,3-triazole tethered isatin-ferrocene conjugates: synthesis and in vitro antimalarial evaluation. Eur J Med Chem. 2014;87:801–4.
28. Domingo LR. Molecular Electron Density Theory: a modern view of reactivity in Organic Chemistry. Molecules. 2016;21(10):1319.
29. Ríos-Gutiérrez M, Domingo LR. Unravelling the mysteries of the [3 + 2] cycloaddition reactions. Eur J Org Chem. 2018;2019(2–3):267–82.
30. Bailly C. Lamellarins, from a to Z: a family of Anticancer Marine Pyrrole alkaloids. Curr Med Chemistry-Anti-Cancer Agents. 2004;4(4):363–78.
31. Bellina F, Rossi R. Synthesis and biological activity of pyrrole, pyrroline and pyrrolidine derivatives with two aryl groups on adjacent positions. Tetrahedron. 2006;62(31):7213–56.
32. Narayan R, Potowski M, Jia Z-J, Antonchick AP, Waldmann H. Catalytic enantioselective 1,3-dipolar cycloadditions of azomethine ylides for biology-oriented synthesis. Acc Chem Res. 2014;47(4):1296–310.
33. Boudriga S, Haddad S, Murugaiyah V, Askri M, Knorr M, Strohmann C, Golz C. Three-Component Access to Functionalized Spiropyrrolidine Heterocyclic Scaffolds and their cholinesterase inhibitory activity. Molecules. 2020;25(8):1963.
34. Barakat A, Soliman SM, Alshahrani S, Islam MS, Ali M, Al-Majid AM, Yousuf S. Synthesis, X-ray single crystal, Conformational Analysis and cholinesterase inhibitory activity of a New Spiropyrrolidine Scaffold Tethered Benzo[b] Thiophene Analogue. Crystals. 2020;10(2):120.
35. Alshahrani S, Al-Majid AM, Ali M, Alamary AS, Abu-Serie MM, Dömling A, Shafiq M, Ul-Haq Z, Barakat A. Rational design, synthesis, separation, and characterization of New spiroxindoles combined with Benzimidazole Scaffold as an MDM2 inhibitor. Separations. 2023;10(4):225.
36. Alshahrani S, Al-Majid AM, Alamary AS, Ali M, Altowyan MS, Ríos-Gutiérrez M, Yousuf S, Barakat A. Synthesis and characterization of New spirooxindoles Including Triazole and Benzimidazole Pharmacophores via [3 + 2] Cycloaddition reaction: an MEDT Study of the mechanism and selectivity. Molecules. 2023;28(19):6976.
37. Calais JL: Density-functional theory of atoms and molecules., Parr RG, Yang W. Oxford University Press, New York, Oxford, 1989. IX + 333 pp. Price £45.00. *International Journal of Quantum Chemistry* 1993, 47(1):101–101.
38. Domingo LR, Ríos-Gutiérrez M, Pérez P. Applications of the conceptual density functional theory indices to Organic Chemistry Reactivity. Molecules. 2016;21(6):748.
39. Domingo LR, Ríos-Gutiérrez M. Application of reactivity indices in the study of Polar < Scp > D iels– <scp > A lder Reactions</scp >. Conceptual density functional theory. Wiley; 2022. pp. 481–502.
40. Parr RG, Pearson RG. Absolute hardness: companion parameter to absolute electronegativity. J Am Chem Soc. 1983;105(26):7512–6.
41. Domingo LR, Ríos-Gutiérrez M, Pérez P. A molecular electron density theory study of the participation of tetrazines in aza-diels-alder reactions. RSC Adv. 2020;10(26):15394–405.
42. Doming LR, Ríos-Gutiérrez M. A useful classification of Organic reactions based on the Flux of the Electron Density. Sci Radices. 2023;2(1):1–24.
43. Parr RG, Szentpály Lv, Liu S. Electrophilicity Index. J Am Chem Soc. 1999;121(9):1922–4.
44. Domingo LR, Chamorro E, Pérez P. Understanding the reactivity of Captodative ethylenes in Polar Cycloaddition reactions. A theoretical study. J Org Chem. 2008;73(12):4615–24.
45. Ríos-Gutiérrez M, Saz Sousa A, Domingo LR. Electrophilicity and nucleophilicity scales at different DFT computational levels. J Phys Org Chem 2023, 36(7).
46. Domingo LR, Ríos-Gutiérrez M, Pérez P. Why is phenyl azide so unreactive in [3 + 2] cycloaddition reactions? Demystifying Sustmann's paradigmatic parabola. Org Chem Front 2023.
47. Ríos-Gutiérrez M, Domingo LR, Jasiński R. Unveiling the high reactivity of experimental pseudodiradical azomethine ylides within molecular electron density theory. Phys Chem Chem Phys. 2023;25(1):314–25.
48. Aurell MJ, Domingo LR, Pérez P, Contreras R. A theoretical study on the regioselectivity of 1,3-dipolar cycloadditions using DFT-based reactivity indexes. Tetrahedron. 2004;60(50):11503–9.
49. Domingo LR, Pérez P, Sáez JA. Understanding the local reactivity in polar organic reactions through electrophilic and nucleophilic Parr functions. RSC Adv. 2013;3(5):1486–94.
50. Domingo LR, Ríos-Gutiérrez M, Barakat A. A Molecular Electron Density Theory Study of the [3 + 2] Cycloaddition reaction of an azomethine ylide with an Electrophilic Ethylene Linked to Triazole and Ferrocene units. Molecules. 2022;27(19):6532.
51. Ríos-Gutiérrez M, Barakat A, Domingo LR. A Molecular Electron Density Theory Study of the [3 + 2] Cycloaddition reaction of Pseudo(mono)radical azomethine ylides with Phenyl Vinyl Sulphone. Organics. 2022;3(2):122–36.

52. Domingo LR, Sáez JA. Understanding the electronic reorganization along the nonpolar [3 + 2] cycloaddition reactions of Carbonyl Ylides. J Org Chem. 2010;76(2):373–9.
53. Fukui K. Formulation of the reaction coordinate. J Phys Chem. 1970;74(23):4161–3.
54. Domingo LR. A new C–C bond formation model based on the quantum chemical topology of electron density. RSC Adv. 2014;4(61):32415–28.
55. Diffraction RO. CrysAlisPro; Rikagu Oxford Diffraction Inc.: Oxfordshire, UK 2022.
56. Sheldrick GM. SHELXT - integrated space-group and crystal-structure determination. Acta Crystallogr Found Adv. 2015;71(Pt 1):3–8.
57. Sheldrick GM. Crystal structure refinement with SHELXL. Acta Crystallogr C Struct Chem. 2015;71(Pt 1):3–8.
58. Hübschle CB, Sheldrick GM, Dittrich B. ShelXle: a qt graphical user interface for SHELXL. J Appl Crystallogr. 2011;44(Pt 6):1281–4.
59. Spackman PR, Turner MJ, McKinnon JJ, Wolff SK, Grimwood DJ, Jayatilaka D, Spackman MA. CrystalExplorer: a program for Hirshfeld surface analysis, visualization and quantitative analysis of molecular crystals. J Appl Crystallogr. 2021;54(Pt 3):1006–11.

Publisher's note